# The crystal structure of isotactic 1,4-trans-poly(2-methylpentadiene). An application of the Rietveld method

4 AUTHORS:

Sergio Brückner
University of Udine
**110** PUBLICATIONS **2,299** CITATIONS

SEE PROFILE

Silvia Luzzati
Italian National Research Council
**71** PUBLICATIONS **1,185** CITATIONS

SEE PROFILE

W. Porzio
Italian National Research Council
**228** PUBLICATIONS **3,030** CITATIONS

SEE PROFILE

Piero Sozzani
Università degli Studi di Milano-Bicocca
**67** PUBLICATIONS **1,321** CITATIONS

SEE PROFILE

siloxanes under consideration, and we add that the role of the main chain has been completely ruled out from our discussion, although it does participate in some manner to the solute–solvent interactions.

This work engages us to proceed in order to clarify the different points discussed above. The forthcoming studies will include the change of the nature of the polymer, first, in order to analyze the influence of the backbone and, second, to avoid neighboring core–core overlaps and to evaluate the importance of this factor on the phase separation. In contrast, the strengthening of this antiparallel arrangement can be obtained with polar side groups attached to the poly(methylsiloxane) backbone. With regard to the solvent, we envision the use of polar solvents, which in turn could show a tendency to antiferroelectric interactions.

**Acknowledgment.** We are greatly indebted to Dr. Nguyen Huu Tinh for the use of the series of mesogenic LMW compounds.

## References and Notes

(1) Arnold, H.; Sackmann, H. *Z. Phys. Chem. (Leipzig)* **1960**, *213*, 137; **1960**, *213*, 145.
(2) Billard, J. *Bull. Soc. Fr. Mineral. Cristallogr.* **1972**, *95*, 206.
(3) Casagrande, C.; Veyssie, M.; Finkelmann, H. *J. Phys. (Paris)* **1982**, *43*, L-671.
(4) Nguyen Huu Tinh; Destrade, C.; Gasparoux, H. *Phys. Lett.* **1979**, *72A*, 251.
(5) Casagrande, C.; Veyssie, M. Presented at the Colloque Polymeres Cristaux Liquides, Nice, France, 1985.
(6) Brochard, F.; Jouffroy, J.; Levison, P. *J. Phys. (Paris)* **1984**, *45*, 1125.
(7) Benthack-Thoms, H.; Finkelmann, H. *Makromol. Chem.* **1985**, *186*, 1895.
(8) Kofler, L.; Kofler, A. Verlag Chemie: Weinheim, 1954.
(9) Sigaud, G.; Hardouin, F.; Achard, M. F. *Proceedings of the 12th Journées d'Etudes des Equilibres entre Phases*; Haget, Y., Ed.; Université de Bordeaux I: Talence, France, 1986.
(10) Sigaud, G.; Achard, M. F., unpublished results.
(11) Hansen, J. P.; McDonald, J. R. *Theory of Simple Liquids*; Academic: London, 1976.
(12) Mauzac, M.; Hardouin, F.; Richard, H.; Achard, M. F.; Sigaud, G.; Gasparoux, H. *Eur. Polym. J.* **1986**, *22*, 137.
(13) Smith, G. W.; Gardlund, Z. G. *J. Chem. Phys.* **1973**, *59*, 3214.
(14) Nguyen Huu Tinh, Presented at the 7th Conference of Socialist Countries, Halle, GDR, 1985.
(15) Nguyen Huu Tinh, private communication.
(16) Nguyen Huu Tinh; Zann, A.; Dubois, J. C. *Mol. Cryst. Liq. Cryst.* **1979**, *53*, 43.
(17) Achard, M. F.; Hardouin, F.; Sigaud, G.; Mauzac, M. *Liq. Cryst.* **1986**, *1*, 203.
(18) We will often refer in the following to the polymer as the solute and to the LMW nematogen as the solvent (since $X_c = 0.1$).

# Crystal Structure of Isotactic 1,4-*trans*-Poly(2-methylpentadiene). An Application of the Rietveld Method

**S. Brückner,*[†] S. Luzzati,[‡] W. Porzio,[‡] and P. Sozzani[§]**

*Dipartimento di Chimica, Politecnico di Milano, P.zza L. da Vinci 32, 20133 Milano, Italy, Istituto di Chimica delle Macromolecole del CNR, via Corti 12, 20133 Milano, Italy, and Dipartimento di Chimica Organica e Industriale, Università di Milano, via Venezian 21, 20133 Milano, Italy. Received July 18, 1986*

ABSTRACT: The crystal structure of isotactic 1,4-*trans*-poly(2-methylpentadiene) has been determined through best fitting of the X-ray diffraction powder profile (Rietveld method). The final refinement cycles were carried out on 12 structural and 18 nonstructural parameters; three constraints were introduced in the form of Lagrange multipliers. A different half-height width for equatorial and layer reflections was adopted in connection with given crystallite dimensions. The final disagreement factor $R_2 = \sum|I_o - I_c|/\sum I_{net}$ was 0.099. The conformation of the polymer chain can be described as a sequence of TS$^+$TS$^-$ torsions. Crystal packing is described, and no particularly short contact is detected.

## Introduction

Crystal structure determinations from powder X-ray diffraction data find at present an increasing number of applications.[1-6] Availability of very accurate experimental data and of efficient computational routines[7,8] that can optimize both structural parameters and parameters that, more generally, depend on experimental conditions of data recording and of sample preparation (e.g., preferred orientation, zero correction, shape of peaks, etc.) is the basis of the recent success of this structural approach, which is usually referred to as the Rietveld[9] whole-fitting method.

In the case of crystalline polymers the analysis of X-ray diffraction data from powders can be convenient when obtaining oriented fibers presents some problem. In fact, in principle, the two-dimensional spreading that characterizes fiber diffraction diagrams allows better resolution among peaks and reveals diffracted intensities at higher $2\theta$ values, thus giving more information. From a practical point of view, however, it is quite often the case that a rigorously quantitative analysis of a powder profile can solve a structural problem in an easier and quicker way, leading to quite reliable results. We have already applied this method to the crystal structure determination of isotactic 1,4-*trans*-poly(1,3-pentadiene) (ITPP),[10] where conflicting conclusions were drawn from an X-ray diffraction analysis from oriented fibers[11] and from a vibrational analysis on a bulk-crystallized sample.[12] Our approach indicated that ITPP assumes different conformations depending on whether crystallization occurs under stretching conditions or not.

The present work is devoted to the study of the crystal structure of isotactic 1,4-*trans*-poly(2-methylpentadiene) (PMPD) (1); Figure 1(II) shows the numbering scheme of
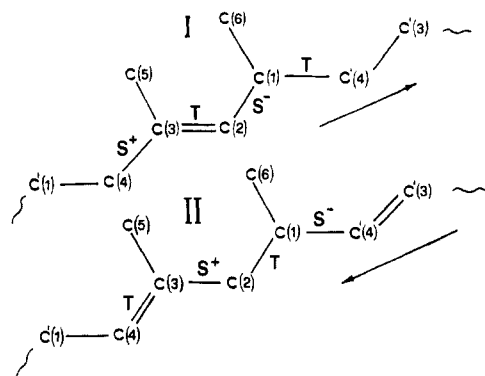
**1**
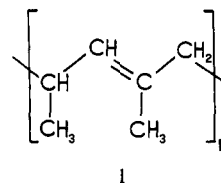
carbon atoms. This polymer has been known for many

[†] Dipartimento di Chimica, Politecnico di Milano.
[‡] Istituto di Chimica delle Macromolecole del CNR.
[§] Dipartimento di Chimica Organica e Industriale, Università di Milano.

**Figure 1.** Schematic view of the chain where it is possible to see that this polymer has a definite direction of propagation and that this direction can be changed by simply relocating the double bond. Numbering scheme II is the one adopted in the final model.

**Table I**
**Experimental Details of X-ray Diffraction Powder Profile Measurement of Isotactic 1,4-*trans*-Poly(2-methylpentadiene)**

| | |
|---|---|
| instrument | Siemens D-500 goniometer equipped with step–scan attachment, proportional counter, and Soller slits, controlled with a Hewlett-Packard computer |
| radiation (power) | Cu Kα, Ni-filtered (40 kV, 30 mA) |
| divergence aperture | 0.3° from 9° to 18° (2θ) and 1° above (rescaling through an overlap margin of 16–18°) |
| receiving aperture | 0.05° |
| step width | 0.05 (2θ) |
| count time | 40 s per step |
| 2θ range | 9–50° |
| temperature | +25 and −120.0 (5) °C (under vacuum (ca. $10^{-3}$ mmHg)) |

**Table II**
**Unit Cell Dimensions Detected from Powder X-ray Diffraction Spectra at +25 and −120 °C**

| +25 °C | −120 °C |
|---|---|
| $a$ = 4.819 (7) Å | $a$ = 4.823 (5) Å |
| $b$ = 9.186 (5) Å | $b$ = 9.084 (3) Å |
| $c$ = 12.891 (6) Å | $c$ = 12.776 (3) Å |
| $\beta$ = 93.5 (10)° | $\beta$ = 93.6 (8)° |
| $V$ = 570 (1) Å³ | |
| $D_c$ = 0.96 g cm⁻³ ($Z$ = 4) | |
| space group $P2_1/c$ | |

years[13] but its crystal structure, to our knowledge, was never determined, probably owing to the very poor quality of X-ray diffraction patterns obtained from oriented fibers; in fact, the dominant contribution to diffraction intensities comes from an oriented paracrystalline phase, and this contribution heavily masks intensities that come from a less oriented crystalline phase. The powder X-ray diffraction profile of PMPD shows, on the contrary, very well-defined peaks up to rather high 2θ values. This is a challenging problem for a structural approach based on the Rietveld method, and we decided therefore to solve the crystal structure of PMPD by fitting its powder X-ray diffraction profile.

## Experimental Section

1,4-*trans*-Poly(2-methylpentadiene) was obtained by inclusion polymerization at room temperature, adding *trans*-2-methyl-1,3-pentadiene (Fluka, puriss. standard) to preirradiated per-hydrotriphenylene (PHTP), as described in ref 14. The PHTP-polymer adduct was decomposed by extraction in boiling pentane. Due to the insolubility of the polymer in common solvents, its microstructure was determined by ¹³C NMR analysis after mild reduction to hemitactic polypropylene.[15] PMPD has a content of isotactic diads of at least 96%[16] and a pure 1,4-trans head-to-tail enchainment, like all pentadienes polymerized in PHTP.[17] The native PMPD melts at 200.6 °C ($\Delta H_f$ = 80 J/g) and, after cooling and reheating at 5 K/min, DSC shows two endothermic transitions at 184 and 190 °C. For powder X-ray diffraction measurements PMPD, sealed in a glass tube under vacuum, was annealed at 187 (1) °C for 48 h in an aluminum oven and then spontaneously cooled in the oven at room temperature. After this treatment the DSC curve shows only one peak at 191 °C ($\Delta H_f$ = 68 J/g).

The bulk polymer was then ground, and the sample holder was filled with the powder thus obtained. X-ray diffraction profiles were recorded at +25 and −125 °C. Low-temperature data were collected in order to minimize the contribution of atomic thermal vibration parameters to the structure factors, thereby enhancing the signal-to-background ratio, particularly at high 2θ values; we refer to the low-temperature spectrum in all comparisons of experimental data. In Table I we summarize the experimental details of data collection.

## Structural Analysis

An oriented fiber X-ray diffraction diagram, though of poor quality, as already stated, was very useful in discriminating between equatorial and layer peaks. Equatorial peaks (0$kl$) were easily indexed in a rectangular lattice whereas some difficulty arose for the definition of the third dimension since only a few well-defined layer peaks can be observed on the powder X-ray diffraction profile (peaks at 24.5, 25.8, and 31.0° on the 2θ scale). Assuming a repeat period of 4.8–4.9 Å along the chain axis, as suggested by both the fiber diagram and the already-

solved structure of ITPP, it was possible to select only two acceptable cells, both of them monoclinic, space group $P2_1/c$ (a guess consistent with the content of the unit cell ($Z$ = 4) and with the few systematic absences that could be detected), and with the same volume, since they differ only in the indexing of layer peaks, which gives a calculated density of 0.96 g cm⁻³ at room temperature. The dimensions of the correct cell are given in Table II at both temperatures. For the sake of brevity we do not describe here details of the optimization procedure carried out with the wrong cell. It may be enough to point out that, though layer peaks are few and weak, it was never possible to reproduce them satisfactorily with the wrong indexing; in particular, the peak at 2θ = 24.5° proved to be very critical with respect to the two possible choices. We point out this finding as an example of the discriminating power of powder X-ray diffraction data with respect to erroneous models.

We used a refinement routine written by Immirzi[8], and partially modified by one of the authors, in order to allow the introduction of geometrical constraints in the structural models in the form of Lagrange multipliers.[18] In this way it is possible to fulfill boundary conditions on geometrical features defined by atoms belonging to adjacent cells, a capability that is particularly useful in the case of chain polymers that propagate from one cell to the adjacent one along the chain axis and where some internal coordinate is necessarily defined by atoms belonging to different cells. A further modification concerns the possibility of defining a specific half-height width for each reflection in connection with given average dimensions of crystallites, according to an analysis due to Perego, Cesari, and Allegra.[19] This capability is particularly useful in this case since, as may be seen in the experimental X-ray diffraction diagram (Figure 2, curve a)), equatorial peaks (e.g., at 2θ = 11.97°, 13.90°, 17.00°, 19.55°, and 20.77°) are much sharper than layer peaks (e.g., at 2θ = 24.50°, 25.81°, and 31.02°). Insofar as we may attribute this differential broadening solely to a difference in crystallite dimensions we expect crystallites to show a lamellar shape with a small thickness along the chain axis.
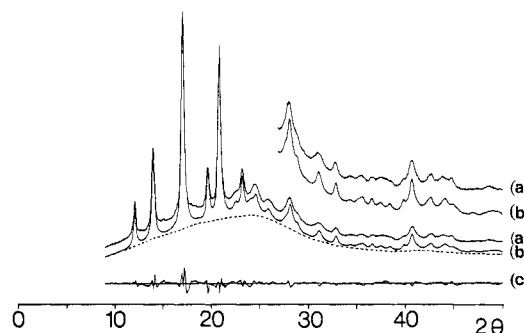
**Figure 2.** The observed X-ray diffraction profile collected at –120 °C (curve a) is compared with the calculated profile (curve B). The dotted line indicates the calculated background profile, while curve c represents the difference profile. Curves a' and b' are the same as curves a and b on an expanded intensity scale. The shifts of the curves along the intensity axis are arbitrary.

A rigid-body model, obtained substantially from the already-solved structure of ITPP with the insertion of an additional side methyl group, was assumed as the starting point of the optimization procedure. Three translations and one rotation around the chain axis were the only adjustable structural parameters in this preliminary analysis. Only a few cycles were sufficient to locate this rigid model in the unit cell so that rather good agreement was observed between calculated and observed equatorial peaks. Layer peaks, however, were not satisfactorily reproduced, and we decided to adopt a more flexible model. All chain bonds were allowed to twist freely under the constraints represented by one bond length (C(1)–C'(4)) and two bond angles (C(3)–C(4)–C'(1) and C'(4)–C(1)–C(2); see Figure 1 (II) for the numbering scheme), which were kept fixed at standard values. Two main-chain bond angles were also allowed to vary. Refinement, carried out with this flexible model, resulted in a wide conformational rearrangement, which took place without affecting appreciably the agreement of equatorial peaks but greatly increasing agreement of layer peaks. What actually happened is shown in Figure 1, where it is possible to see that this chain has a definite direction of propagation, thus allowing for two possible insertions at a given position in the unit cell. Figure 1 also shows that it is possible to reverse a given direction by simply relocating the double bond (from C(2)=C(3) to C(3)=C(4)) without modifying connections involving side-chain methyl groups. The conformational rearrangement observed by us actually corresponds to a relocation of the double bond, and, in fact, the torsion angle around C(3)–C(4) changed from S$^+$ to T while the torsion angle around C(2)–C(3) (which was originally considered a double bond) changed from T to S$^+$. The remaining two main-chain bonds changed correspondingly. The *y,z* coordinates of the side-chain methyl groups did not change substantially in this new conformation.

It should be stressed here that even if this finding may be not so important in view of the final result (actually the same conclusion could have been reached by simply inverting the direction of the rigid model), it is important, in our opinion, from a methodological point of view since it shows that powder diffraction data can drive a suitably flexible model toward a correct position in the cell through changes that are well beyond what is usually considered a "refinement" of structural parameters.

A subsequent readjustment of some bond lengths and angles and of some hydrogen atoms completed the conversion to the new model. The final refinement was performed over 12 structural parameters under the action of the three constraints already mentioned, acting on one

**Table III**
**Disagreement Factors**

| region A$^c$ | region B$^d$ | total | $\chi^2/(N - P)^b$ |
|---|---|---|---|
| 0.087 | 0.128 | 0.099 | 3.0 |

$R_2 = \sum|I_o - I_c|/\sum I_{net}{}^a$

$^a I_{net} = I_o - I_{backgr}.$  $^b N$ is the number of profile points (820); $P$ is the total number of refinable parameters; $\chi^2 = \sum w(I_o - I_c)^2$; $w$ is the weight factor.  $^c 3.6 < d \le 9.8$ Å, $9° \le 2\theta < 25°$.  $^d 1.8 < d \le 3.6$ Å, $25° \le 2\theta < 50°$.

**Table IV**
**Final Fractional Coordinates of Carbon and Hydrogen Atoms Together with Conformational Features**$^a$

| atom | x | y | z |
|---|---|---|---|
| C(1) | -0.5681 (70) | 0.2937 (26) | 0.1565 (36) |
| C(2) | -0.3519 (70) | 0.4171 (21) | 0.1646 (19) |
| C(3) | -0.0645 (69) | 0.3587 (18) | 0.1893 (9) |
| C(4) | 0.1489 (84) | 0.3568 (41) | 0.1258 (24) |
| C(5) | -0.0133 (127) | 0.3145 (62) | 0.3020 (16) |
| C(6) | -0.5067 (120) | 0.1750 (52) | 0.0750 (58) |
| H(1) | 0.118 (11) | 0.399 (9) | 0.055 (7) |
| H(2) | -0.571 (10) | 0.241 (5) | 0.232 (4) |
| H(3) | -0.357 (8) | 0.476 (3) | 0.091 (3) |
| H(4) | -0.404 (8) | 0.493 (3) | 0.226 (3) |
| H(5) | -0.098 (16) | 0.206 (6) | 0.313 (4) |
| H(6) | -0.114 (16) | 0.393 (8) | 0.351 (3) |
| H(7) | 0.208 (14) | 0.314 (9) | 0.322 (4) |
| H(8) | -0.401 (17) | 0.225 (9) | 0.012 (5) |
| H(9) | -0.700 (15) | 0.127 (6) | 0.044 (7) |
| H(10) | -0.377 (11) | 0.091 (4) | 0.112 (9) |

Conformational Features:  Bond Lengths, Bond Angles, and Torsion Angles

Bond Lengths (Å)

| | | | | | |
|---|---|---|---|---|---|
| C(1)–C(2) | 1.53 | C(2)–C(3) | 1.50 | C(3)–C(4) | 1.35 |
| C(3)–C(5) | 1.50 | C(1)–C(6) | 1.54 | C(1)–C'(4) | 1.51 |

Bond Angles$^b$ (Deg)

| | | | |
|---|---|---|---|
| C'(4)–C(1)–C(2) | 110 | C(2)–C(3)–C(5) | 113 (2) |
| C(1)–C(2)–C(3) | 112 | C(3)–C(4)–C'(1) | 124 |
| C(4)–C(3)–C(5) | 119 (2) | C(2)–C(1)–C(6) | 113 (1) |
| C'(4)–C(1)–C(6) | 107 (2) | C(2)–C(3)–C(4) | 127 (2) |

Torsion Angles (Deg)

| | | | |
|---|---|---|---|
| C'(3)–C'(4)–C(1)–C(2) | -113 (2) | C'(4)–C(1)–C(2)–C(3) | -177 (2) |
| C(1)–C(2)–C(3)–C(4) | 111 (3) | C(2)–C(3)–C(4)–C'(1) | 181 (2) |
| C(1)–C(2)–C(3)–C(5) | -76 (2) | C(3)–C(2)–C(1)–C(6) | -57 (2) |
| C'(3)–C'(4)–C(1)–C(6) | 123 (2) | C'(1)–C(4)–C(3)–C(5) | 8 (2) |

$^a$ Thermal factors were not refined; they are 0.5 and 2.0 Å$^2$ for carbon and hydrogen atoms, respectively (at $T$ = -120 °C).  $^b$ Bond angles without esd's were not refined.

bond length and two bond angles. Only at the very end of the procedure were torsion angles of side-chain methyl groups slightly adjusted to improve agreement with the observed profile. In Figure 2 we report a comparison between experimental (curves a and a') and calculated (curves b and b') profiles together with the difference profile (curve c) and background (dotted line). In Table III we report the final disagreement factors $R_2 = \sum|I_o - I_c|/\sum I_{net}$ and $\chi^2/(N - P)$; for the former, in addition to the total, we also report two partial values corresponding roughly to the region of large peaks (region A; $9° < 2\theta < 25°$) and the region of small peaks (region B; $25° < 2\theta < 50°$).

**Discussion**

Final values of positional and nonpositional refined parameters are reported, separately, in Tables IV and V, respectively. Positional parameters are reported together with bond lengths, bond angles, and torsion angles for a complete definition of chain conformation in the crystalline state.

**Table V**
**Refined Nonstructural Parameters**

| | |
|---|---|
| zero correction $2\theta$, deg | −0.125 (5) |
| preferred orientation[a] | $G = 0.027$ (9); indices [100] |
| profile function parameters[b] | |
| $U$ | 0 |
| $V$ | 0.232 (8) |
| $W$ | different for each reflection (see text) |
| $m$ | 1 |
| intensities ($k$ counts) of the points on the segmented line | |
| $2\theta = 9.0°$ | 0.691 (10) |
| $2\theta = 14.0°$ | 2.155 (12) |
| $2\theta = 18.6°$ | 2.901 (17) |
| $2\theta = 38.0°$ | 1.794 (8) |
| $2\theta = 50.0°$ | 1.696 (5) |

Bell-Shaped Curves[c]

| no. | int/1000 | width, deg | $2\theta$, deg | $m$ |
|---|---|---|---|---|
| 1 | 2.74 (10) | 9.8 (2) | 25.24 (5) | 1.5 |
| 2 | 0.37 (7) | 4.8 (4) | 42.13 (18) | 1.5 |

[a] Preferred orientation factor PO = $\exp(-G\alpha_k^2)$; $\alpha_k$ is the angle between the scattering vector of the $k$th reflection and the scattering vector of a fixed (the preferred) reflection. [b] According to the relation $H_k^2 = U \tan^2 \theta_k + V \tan \theta_k + W$; $m$ is the exponent in the Pearson profile function $f(z) = (C/H_k)[1 + 4(2^{1/m} - 1)z^2]^{-m}$, with $z = (2\theta_i - 2\theta_k)/H_k$. [c] $K\alpha_1 - K\alpha_2$ splitting was taken into account. The bell-shaped curves of the background are again a Pearson distribution, but with $m = 1.5$.

First, we make a few comments on the nonstructural parameters. Superposition of (i) a large bell-shaped curve (centered at $2\theta = 25.2°$), of (ii) a secondary small one (centered at $2\theta = 42.1°$), and of (iii) a segmented line crossing five points gives rise to the optimized base line shown in Figure 2 (dotted line). Parameters defining the bell-shaped curves and the five points on the segmented line are reported in Table V. In particular, we point out that only the intensities of the five points are refinable while their location on the $2\theta$ scale is *not* adjustable. Strictly speaking, the portion of the spectrum below the base line contains all that *cannot* be explained by our crystalline model. Since it gives rise to a smooth curve showing a rather reasonable path with a broad maximum at ca. $2\theta = 25°$, we did not undertake any further investigation of it from the experimental point of view. Rather small effects of preferred orientation of crystallites and of zero correction on the experimental $2\theta$ scale had to be taken into account. Peak shapes are described by Pearson VII distributions with $m = 1$ (Cauchy distributions),[20] while, as previously mentioned, it was found necessary to adopt quite different half-height widths $H_k$ for equatorial and layer peaks. Both kinds of peaks show substantially the same dependence of $H_k$ on $\theta$, expressed as $H_k^2 = W + V \tan \theta$, with the same coefficient $V$, reported in Table V, while strong differences are detected on $W$, which is of the order of 0.07 for equatorial peaks and of the order 0.40 for layer peaks. When these values are used to obtain $H_k$ ($\cong 0.30°$ and $\cong 0.65°$, respectively, at low $2\theta$ values), it is possible to estimate the average dimensions of crystallites through the application of eq 15 and 16 of ref 19. These equations are strictly valid only in the case of peak shapes described by a Cauchy distribution and give results that are lower than those obtainable through the classical Scherrer approach. It is necessary, of course, to take into account instrumental broadening, which was determined to be less than 0.1° (by recording spectra of products with high average crystal size, as quartz and $\alpha$-Al$_2$O$_3$), corresponding to a fictitious crystallite dimension greater then 250 Å over the whole $2\theta$ range considered. Once this
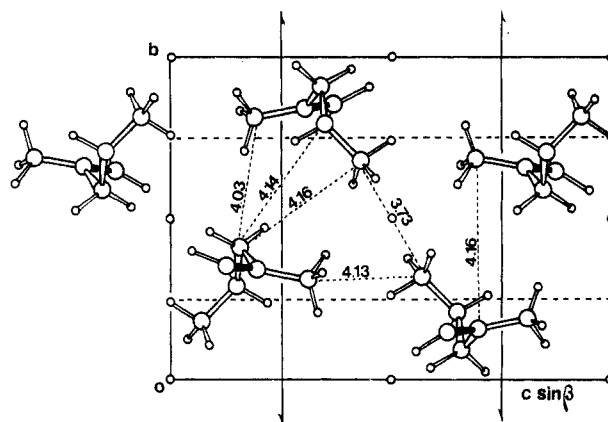


**Figure 3.** Chain packing viewed along the $a$ axis. Only the shortest interchain contacts are reported.

correction is introduced, we obtain indication of the presence of rather flat crystallites of about 50 × 160 × 160 Å with the shortest dimension along the chain axis. The chain conformation can be described as a sequence of TS$^+$TS$^-$ torsions, as shown in Table IV, and is quite close to the one expected for this polymer. Observed skew torsions of PMPD (S$^+$ = 111° and S$^-$ = −113°) deviate less than 10° from theoretical values of ±120°, but in the opposite direction of that observed in the case of ITPP, where skew torsions were of the order of ±135° with a difference of ca. 25° from the present conformation. This indicates that the minimum in the potential energy surface corresponding to the region of skew torsions is expected to be rather broad. Bond angles are within acceptable ranges while bond lengths were not refined and therefore have standard values. Packing is shown in Figure 3, viewed along the chain axis $a$; unlike ITPP, in this case the shortest interchain contacts involve main-chain atoms as well as methyl groups. The shortest contact (3.73 Å), however, is between side-chain methyl groups and, though quite acceptable, it is the only critical feature of the present chain packing.

A final remark concerns the coexistence of chains with opposite configurations on tertiary carbon atoms within the same unit cell. This leads to the practical conclusion that if it were possible to synthesize the optically active polymer *of the same microstructure and sufficient purity*, it should crystallize with a different space group. However, in the field of inclusion polymerization,[21] asymmetric induction by optically active PHTP is not high enough. On the other hand, (+)deoxycholic acid (DCA) and (+)apocholic acid (ACA) lead to a lower content in $m$ diads.

**References and Notes**

(1) Young, R. A.; Mackie, P. E.; Von Dreele, R. B. *J. Appl. Crystallogr.* **1977**, *10*, 262.
(2) Young, R. A.; Lundberg, J. L.; Immirzi, A. Proceedings of the ACS Symposium on Diffraction Methods for Structure Determination of Fiber Polymers, Washington, D.C., 1979.
(3) Young, R. A. Main lecture at the 13th International Congress of Crystallography, Hamburg, 1984, and collected abstracts in section "Advances in Powder Diffraction".
(4) Clearfield, A.; McCusker, L. B.; Rudolf, P. R. *Inorg. Chem.* **1984**, *23*, 4679.
(5) Rudolf, P.; Clearfield, A. *Acta Crystallogr., Sect. B: Struct. Sci.* **1985**, *B41*, 418.
(6) Immirzi, A. *Gazz. Chim. Ital.* **1980**, *110*, 381.
(7) Wiles, D. B.; Young, R. A. *J. Appl. Crystallogr.* **1981**, *14*, 149.

(8) Immirzi, A. *Acta Crystallogr., Sect. B: Struct. Sci.* 1980, *B36*, 2378.

(9) Rietveld, H. M. *Acta Crystallogr.* 1967, *22*, 151. Rietveld, H. M. *J. Appl. Crystallogr.* 1969, *2*, 65.

(10) Brückner, S.; Di Silvestro, G.; Porzio, W. *Macromolecules* 1986, *19*, 235.

(11) Bassi, I. W.; Allegra, G.; Scordamaglia, R. *Macromolecules* 1971, *4*, 575.

(12) Neto, N.; Muniz-miranda, M.; Benedetti, E. *Macromolecules* 1980, *13*, 1302.

(13) Cuzin, D.; Chauvin, Y.; Lefebvre, G. *Eur. Polym. J.* 1969, *5*, 283.

(14) Farina, M.; Pedretti, U.; Gramegna, M. T.; Audisio, G. *Macromolecules* 1970, *3*, 475.

(15) Farina, M.; Di Silvestro, G.; Sozzani, P. *Macromolecules* 1982, *15*, 1451.

(16) Di Silvestro, G.; Sozzani, P.; Savarè, B.; Farina, M. *Macromolecules* 1985, *18*, 928.

(17) Sozzani, P.; Di Silvestro, G.; Grassi, M.; Farina, M. *Macromolecules* 1984, *178* 2532.

(18) See, e.g.: Tadokoro, H. In *Structure of Crystalline Polymers*; Wiley: New York, 1979.

(19) Perego, G.; Cesari, M.; Allegra, G. *J. Appl. Crystallogr.* 1984, *17*, 403.

(20) Hall, M. M., Jr. *J. Appl. Crystallogr.* 1977, *10*, 66.

(21) Farina, M. In *Inclusion Compounds*; Atwood, J. L.; Davies, J. E. D., MacNicol, D. D., Eds.; Academic: London, 1984; Vol. 3, Chapter 10.

# Calculation of Induced Circular Dichroism of Acridine Orange–Poly(riboadenylic acid) Complexes and Confirmation of Their Structure

## Toyoko Imae,* Shoji Hayashi, and Shoichi Ikeda

*Department of Chemistry, Faculty of Science, Nagoya University, Chikusa, Nagoya 464, Japan. Received May 8, 1986*

ABSTRACT: Visible circular dichroism induced in acridine orange–poly(riboadenylic acid) complexes has been calculated on the basis of exciton theory to zeroth- and first-order perturbations, assuming an appropriate helical structure and geometry of the complexes. The calculated circular dichroism has been compared with the observed value. The most favorable values of the geometrical parameters for intercalated dyes, half-intercalated dyes, and externally associated dyes have been determined as follows: for the $^1L_b$ transition dipole of the dye chromophore, its polar angle is 80–90° from the poly(riboadenylic acid) helix axis and its azimuthal angle is 90–130° in the plane perpendicular to a helix axis, while its radial distance from the helix axis is 3 Å for the intercalation, 6.0–7.5 Å for the half-intercalation, and 12 Å for the external association, irrespective of whether the strand is double or single. Better agreement is obtained between the calculated and observed circular dichroism when the shape of the absorption band is chosen for the corresponding circular dichroism band, instead of a Gaussian shape, and when the unperturbed band position of circular dichroism is shifted by 5–10 nm toward the blue or red.

## Introduction

We have previously measured absorption spectra and induced circular dichroism of aqueous solutions of acridine orange mixed with poly(riboadenylic acid) [poly(rA)] and reported that acridine orange interacts with poly(rA) in different ways, depending on the pH of the solution and the mole ratio, [P]/[D] (nucleotide residue/added monomeric dye).[1]

At acid pH, where poly(rA) is in a double-stranded helix conformation,[2-5] four kinds of binding modes are successively manifested as the mixing ratio is decreased. Two of them are assigned to intercalation of monomeric dye molecules between base pairs, the first being of dye molecules isolated from the others, and the second being of dye molecules with mutual coupling at neighboring sites. The third is the formation of half–intercalated dimers,[6,7] which consist of a partly intercalated monomer molecule and another monomer molecule incompletely overlapped with it. The fourth is external association of dimeric dye molecules stacked in an antiparallel way.[8]

At neutral pH, where poly(rA) is single-stranded,[3-5,9] isolated intercalation of monomeric dye molecules can occur at the helical parts of poly(rA) when a small amount of dye is added. At intermediate mixing ratios, half-intercalated dimeric dye molecules are bound to adjacent sites. In the presence of excess dye, dimeric dye molecules of the antiparallel type are externally associated with poly(rA).

Two types of mechanisms have been considered to be operative for the induction of optical activity in a symmetrical dye bound to a polynucleotide.[10] The first mechanism involves electronic coupling between dye molecules bound to neighboring sites arranged in a helical manner along the polynucleotide chain, which induces a conservative pair of circular dichroic bands on both sides of the absorption band of the dye. In an alternative mechanism, a bound dye molecule undergoes a dissymmetric perturbation from the nucleotide bases in a helical conformation, inducing a nonconservative circular dichroic band at the wavelength of the absorption band of the dye.

Such induced circular dichroism can be calculated on the basis of the exciton theory of Moffitt, Fitts, and Kirkwood[11] and Tinoco.[12] We have evaluated the circular dichroism of acridine orange bound to DNA by means of the exciton theory of zeroth-order perturbation, which gives a conservative pair of circular dichroic bands associated with dipole–dipole coupling between bound dyes arranged helically.[13]

In this work, we calculate a conservative pair of circular dichroism bands induced in the acridine orange–poly(rA) complex in terms of the zeroth-order perturbation theory, assuming appropriate structures for the complex. Moreover, the present calculation is extended to the treatment of the first-order perturbation by taking account of the dipole–dipole interaction of the electronic transition of the bound dye with another transition of the dye or with